JOURNAL OF MATERIALS SCIENCE 25 (1990) 3297–3308

Preparation and densification of superconducting $YBa_2Cu_3O_x$ ceramics

HUNG C. LING
AT&T Bell Laboratories, Princeton, New Jersey 08540, USA

The solid-state reaction method to form the superconducting oxide $YBa_2Cu_3O_x$ was studied. It was found that the starting cupric and yttrium components accelerated the decomposition of the $BaCO_3$ component. At a constant heating rate of 10° C min^{-1} in thermogravimetric analysis, the temperature of complete decomposition, T_f, was lowered from greater than 1000° C in pure $BaCO_3$ to between 915 and 985° C. The effectiveness in decreasing T_f can be ranked in the order of oxalate, carbonate and oxide. The highest sintered density achieved in this study was 6.03 g cm^{-3} (ρ/ρ_{th} = 95%) at 990° C and 5.85 g cm^{-3} (ρ/ρ_{th} = 92%) at 960° C. The source of cupric ion had the largest effect on densification. The use of cupric carbonate resulted in a consistently high Archimedes density of about 6.00 g cm^{-3} and large dimensional shrinkage of about 20% at 990° C for 12 h. In contrast, the use of cupric oxide gave the lowest density and smallest shrinkage. Within the same powder lot, higher sintered density and smaller dimensional shrinkage were observed in samples with higher initial green density and compaction pressure. However, the data suggested that the enhanced densification and higher density achieved by the use of cupric carbonate and oxalate cannot be accounted for by the different physical characteristics of the powders and the mechanics of powder compaction, measured collectively by the green density.

1. Introduction

The solid-state reaction method to form the superconducting ceramic $YBa_2Cu_3O_x$ has generally involved the use of barium carbonate ($BaCO_3$), yttrium oxide (Y_2O_3) and cupric oxide (CuO) [1–11]. The sintered densities of compacted samples from these powders were generally quite low, varying between 60 and 85% of the theoretical density. The actual sintered density achieved appeared to depend on the powder processing method used by the different groups. For example, by using repeated calcination and milling steps to ensure complete decomposition of raw materials and small particle size after calcination, the sintered density may be increased to over 90% of the theoretical density [1]. Alternatively, hot deformation techniques [2, 4, 12], such as forging or hot isostatic pressing, were employed to produce dense superconducting ceramics. There were also reports on chemically prepared powders with smaller particle size, which sintered to densities between 75 and 95% of theoretical density [13, 14].

It is believed that one main reason for the poor sintering characteristic of the powders derived from the solid-state reaction method is the slow and incomplete decomposition of $BaCO_3$ below 1000° C. Since sintering of the calcined powder must be below the incongruent melting temperature of $YBa_2Cu_3O_x$ (~ 1025° C), calcination is typically performed in the temperature range between 900 and 1000° C for a long period of time. As a result, hard and coarse powders are formed after calcination, requiring a secondary "high energy" milling step to produce an active powder with reduced particle size for sintering. In this paper, the impact of starting copper and yttrium sources on the decomposition of $BaCO_3$ and the subsequent densification of $YBa_2Cu_3O_x$ ceramic during sintering will be examined.

2. Experimental procedures

In this study, $BaCO_3$ was used solely as the source of barium so that water could be used as the mixing and milling medium. For the other metal ions, copper and yttrium, the oxide, carbonate or oxalate of these metals was chosen as the source and constituted one major variable in the study.

A standard powder processing procedure was adopted. Appropriate weight ratios of $BaCO_3$ and the cupric and yttrium ion sources were mixed in a 1000 ml plastic bottle and ball-milled for 4 h in deionized water using ZrO_2 milling medium. The slurry was then filtered and dried at 125° C for 16 h. Prior to calcination, the dried mix was granulated through a 20-mesh screen. Approximately 100 g batches were calcined at 900° C for 2 h, removed and allowed to cool outside the furnace, granulated and re-calcined at 900° C for another 2 h. The calcined powder was granulated using mortar and pestle prior to compaction. Some powders made from a combination of barium carbonate, cupric oxide and yttrium oxide (lot E1350) were also calcined at 950° C for 16 h. These powders were quite hard and were subjected to a 4 h secondary ball-milling using zirconia balls and isopropanol.

Samples were dry-pressed from the powders in the

0022–2461/90 $03.00 + .12

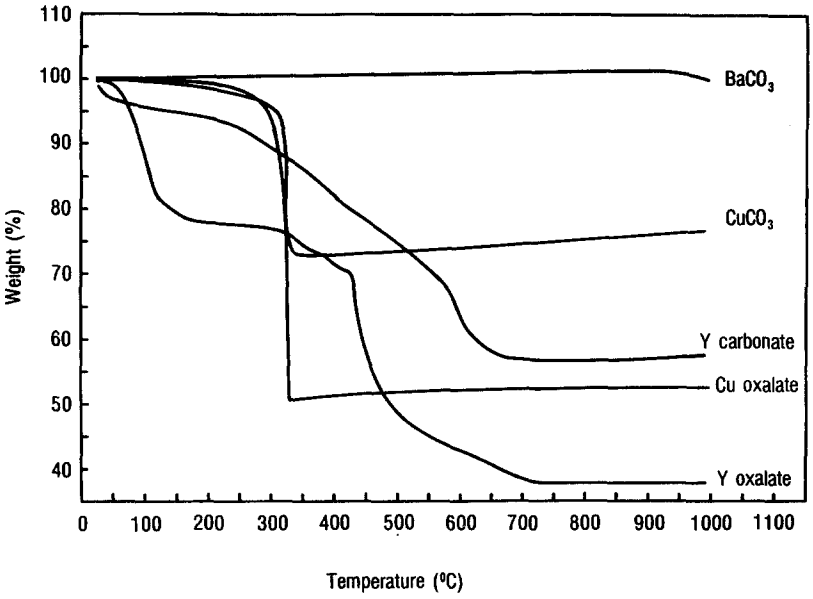

Figure 1 TGA of the starting raw materials: barium carbonate, cupric carbonate, cupric oxalate, yttrium carbonate and yttrium oxalate (heating rate: 10° C min^{-1}).

form of 0.5 in (1.27 cm) diameter discs, 0.25 in (0.64 cm) diameter discs or rectangular bars measuring 0.125 in (0.32 cm) in width and 0.5 in (1.27 cm) in length under an average pressure of 24 000 psi (165.5 MPa) or 15 000 psi (103.4 MPa). The samples were heated at a rate of 400° C h^{-1} to a temperature between 960 and 990° C and sintered for 5 min, 1 h, 3 h or 12 h in oxygen. All the sintering runs were followed by annealing at 550° C for 2 h and slow cooling to room temperature. The variation in sintering temperature and time constituted the second major variable, in addition to the variable of starting copper and yttrium sources.

The geometrical densities were determined from the weight and the physical dimensions of the samples after sintering. For dense samples, the Archimedes densities were determined by the submersion method, using carbon tetrachloride as the liquid medium. Dimensional shrinkage was calculated from the change in radius of the disc samples or from the average change in the length and the width of the bar samples before and after sintering. Electrical resistance was measured using the four-point technique from room temperature to 77 K. Magnetic susceptibility was measured between room temperature and 77 K at 13 Hz and under an applied field of 1 G. X-ray diffraction patterns were obtained from the calcined powders as well as the sintered discs using filtered copper radiation. Thermogravimetric analysis (TGA) of the starting materials and the powder lots before calcination was performed to determine the temperature range of decomposition. TGA was done in flowing air at a constant heating rate of 10° C min^{-1}.

3. Results and discussion

3.1. Thermogravimetric analysis

The TGA of the starting materials: barium carbonate, yttrium oxalate, yttrium carbonate, cupric oxalate and cupric carbonate is shown in Fig. 1. In the ball-milled powders prior to calcination, the decomposition characteristics of the individual components were preserved in their respective temperature ranges. As an example, Fig. 2a shows the TGA curves of three powder lots: E1314, E1306 and E1329. In this series, $BaCO_3$ and yttrium oxalate were used in combination with cupric oxide (E1314), cupric carbonate (E1306) or cupric oxalate (E1329). The cupric sources were decomposed by 350° C, the yttrium oxalate by 700° C while the temperature at which $BaCO_3$ was completely decomposed. T_f, was at 955° C for E1314, 930° C for E1306 and 915° C for E1329. Fig. 2b shows the corresponding TGA curves for a combination of barium carbonate and yttrium oxide with cupric oxide (E1305), cupric carbonate (E1309) and cupric oxalate (E1328). $BaCO_3$ was again all decomposed below 1000° C. In contrast, there was very little decomposition of pure $BaCO_3$ at 1000° C, with a measured weight loss of only 1.3%.

In all the powder lots, the decomposition of the $BaCO_3$ component started around 800° C, but the temperature at which the decomposition was completed, T_f, was affected by the starting yttrium and copper sources. Table I lists T_f and the measured weight loss due to the decomposition of $BaCO_3$ component, together with the calculated weight loss based on the percentage of $BaCO_3$ in the powder lots. The measured weight loss agreed very well with the calculated weight loss to within 0.5%, except for lot E1305 where 1.3% was retained. This indicated that at temperatures above 955° C, the decomposition of the $BaCO_3$ component was completed in most of the powder lots in this study. A small amount of $BaCO_3$ remained above 985° C in lot E1305, which consisted of the most widely used components of cupric oxide and yttrium oxide in addition to $BaCO_3$.

The weight loss of pure $BaCO_3$ at 1000° C was only 1.3% at a constant heating rate of 10° C min^{-1}. Even when a small quantity (~ 0.5 g) of pure $BaCO_3$ was calcined at 1000° C for 2 h, the total weight loss was only 12.7%. This was smaller than the calculated weight loss of 22.3% if the decomposition was complete. Thus, the accelerated decomposition of $BaCO_3$ in the presence of the other components is a significant result. The effectiveness in lowering the decomposition temperature of $BaCO_3$ can be ranked in the order of oxalate, carbonate and oxide regardless of whether

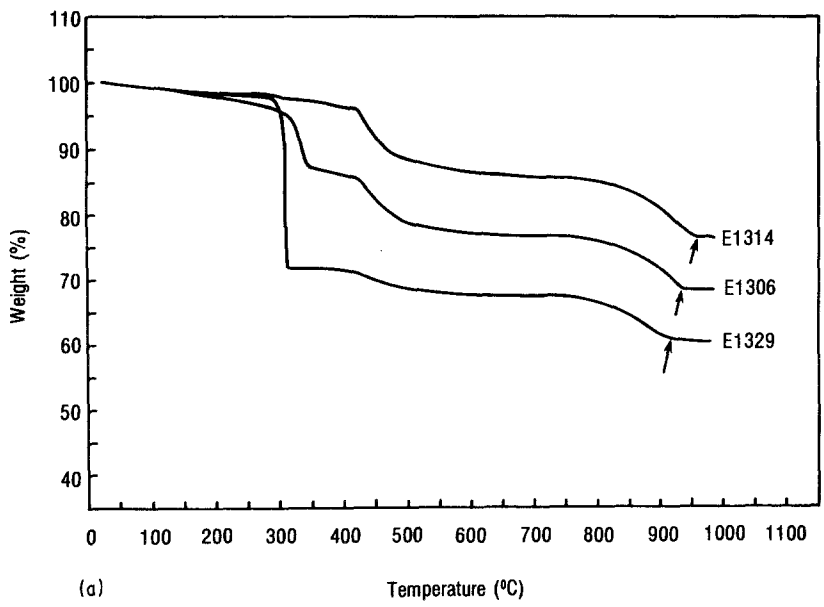

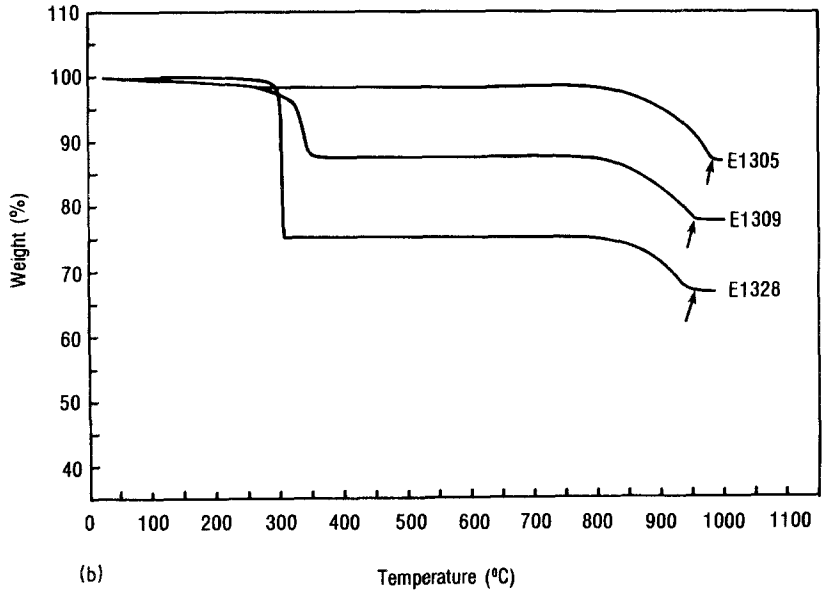

Figure 2 (a) TGA of as-mixed powders: $BaCO_3$ and yttrium oxalate in combination with cupric oxide (E1314), cupric carbonate (E1306) or cupric oxalate (E1329); (b) $BaCO_3$ and yttrium oxide in combination with cupric oxide (E1305), cupric carbonate (E1309) or cupric oxalate (E1328).

TABLE I Weight loss due to decomposition of barium carbonate ($BaCO_3$)

Lot	T_f (°C)*	Measured loss (%)	Calculated loss (%)	$\Delta^\dagger$ (%)	Source
E1305	985	10.5	11.8	1.3	Y oxide, Cu oxide
E1309	955	9.9	10.4	0.5	Y oxide, Cu carbonate
E1328	955	8.0	8.3	0.3	Y oxide, Cu oxalate
E1314	955	9.1	9.4	0.3	Y oxalate, Cu oxide
E1306	930	8.3	8.5	0.2	Y oxalate, Cu carbonate
E1329	915	7.0	7.0	0	Y oxalate, Cu oxalate
E1328	955	8.0	8.3	0.3	Y oxide, Cu oxalate
E1331	925	7.3	7.6	0.3	Y carbonate, Cu oxalate
E1329	915	7.0	7.0	0	Y oxalate, Cu oxalate
E1309	955	9.9	10.4	0.5	Y oxide, Cu carbonate
E1330	955	9.5	9.4	−0.1	Y carbonate, Cu carbonate
E1306	930	8.3	8.5	0.2	Y oxalate, Cu carbonate
Pure $BaCO_3$	1000‡	1.5	22.3	20.7	

*T_f is the temperature at which decomposition of $BaCO_3$ is completed.
†Δ = calculated loss − measured loss.
‡Maximum temperature reached in the TGA analysis.

yttrium or copper source was involved. The lowest T_f of 915° C was attained in lot E1329, which was comprised of $BaCO_3$, yttrium oxalate and copper oxalate.

For the sintering study, the calcination temperatures of all powder lots were fixed at 900° C for 4 h with the exception of a small batch of E1305 that was calcined at 950° C for 16 h. Based on the continuous TGA analysis, a small amount of $BaCO_3$ may have been retained in the calcined powders. The retained amount would be smaller in powders with a lower T_f determined in the TGA. Furthermore, the exact amount would depend on the kinetics of decomposition at 900° C and would be affected by the atmosphere, layer thickness in the calcination boats, etc. In powders using $BaCO_3$, cupric oxide and yttrium oxide as the ingredients, a higher calcination temperature and longer calcination time will be necessary to completely decompose the $BaCO_3$. Otherwise, the remaining $BaCO_3$ could cause poor sintering due to evolution of CO_2 during sintering.

3.2. X-ray analysis

X-ray diffraction was used to determine the quality of the powder lots after sintering. Fig. 3 shows the X-ray diffraction patterns between 2θ angles of 15 and 60° of three series of powder lots. The diffraction patterns were taken from as-sintered surfaces whose compositions are given in the caption to Fig. 3.

Series B powder lots (Fig. 3b) gave the single-phase $YBa_2Cu_3O_x$ pattern when sintered between 960 and 990° C. While series A powder lots (Fig. 3a) showed predominately the $YBa_2Cu_3O_x$ phase, there were a number of additional weak diffraction peaks between 2θ values of 28 and 32°. These small peaks were unidentified and were still present in samples sintered at 1000° C. However, $BaCO_3$ peaks were not detected. Series C powder lots (Fig. 3c) gave more complicated diffraction patterns in which the $YBa_2Cu_3O_x$ lines were diminished in intensity while other extraneous diffraction peaks had increased in intensity. This indicated that multiple phases were formed. Based on the X-ray data, one can conclude that the use of cupric carbonate in place of cupric oxide in the series B powder lots caused the most complete reaction to form the superconducting $YBa_2Cu_3O_x$ phase. The use of cupric oxalate is less desirable due to the formation of multiple phases.

In Fig. 3a, the as-sintered surface of E1305 showed c-axis preferred orientation. This characteristic was present in samples from this lot sintered between 950 and 1000° C. However, the preferred orientation existed only on the surface of the sintered samples. After removing about 40 μm of the surface layer by polishing, the c-axis preferred orientation disappeared and the relative intensities of the diffraction peaks were similar to those obtained on as-sintered disc samples pressed from the other powder lots. The mechanism behind the formation of preferred orientation in lot E1305 is still under investigation. Since c-axis preferred orientation in thin films were observed to give high critical current densities [12–15], understanding the formation mechanism in lot E1305 may shed some light in attacking the low J_c problem in bulk ceramics.

3.3. Sintered density

Fig. 4 shows the normalized electrical resistance of samples sintered at 990° C for 12 h. Among the four lots E1305, E1306, E1309 and E1314, the onset temperature for the superconducting transition was between 90 and 95 K, while zero resistance was reached at temperatures between 87 and 92 K. Thus, all the samples were superconducting above the liquid nitrogen temperature. However, there was a substantial difference in the densification behaviour and the highest density reached among the powders prepared using different starting cupric and yttrium sources.

In bulk ceramics, the sintered density has a tremendous influence on the mechanical properties. The electrical, magnetic or superconducting properties may also be affected to different degrees by the bulk density. An accurate way of measuring the bulk density is by the submersion method based on the Archimedes principle. However, it is only applicable to samples with no open porosity. The alternative, and less accurate, parameter is the geometrical density determined by the weight and the physical dimensions of the sample. In studying the superconductivity phenomenon, a general parameter is required to describe the quality of the sintered ceramic, from porous to dense samples. Thus, the geometrical density was chosen as the parameter to correlate the densification characteristics, measured by the linear shrinkage of samples undergoing different heat treatments.

Fig. 5 shows the correlation between the Archimedes and the geometrical densities for relatively dense samples. The plot represents the aggregate data from four different powder lots and two different sample geometries (discs and rectangular bars). Samples with higher densities were sintered at the higher temperatures and for longer times. As one might expect, an approximately linear relation existed between the geometrical and Archimedes densities. Using a theoretical density of 6.35 g cm^{-3}, the Archimedes density as a percentage of the theoretical density (ρ/ρ_{th}) is also labelled on the right abscissa. For ρ/ρ_{th} greater than 87% (or $\rho > 5.5$ g cm^{-3}), the Archimedes density gave a good measure of the bulk density. If the geometrical density was smaller than ~ 5.0 g cm^{-3}, bubbling was observed when the sample was immersed in the fluid and the Archimedes density remained at about 5.5 g cm^{-3}. The highest density achieved in this study was 95% of theoretical density. This is higher than the typical values of 60 to 85% reported in the literature for powders made by the solid-state reaction route.

Conventional sintering theory of ceramics suggests that there is no open porosity when the bulk density reaches about 95% of the theoretical density. In the case of $YBa_2Cu_3O_x$, the lower limit shifted to 87% in this study. There are two possible causes. It may indicate that sintering on the surfaces of the compacted samples was more rapid than the interior so that internal pores were closed off during the sintering process. Or it may mean that gas evolution prevents the complete sintering internally while, on the surface, gas can escape to allow for full densification. Fig. 6

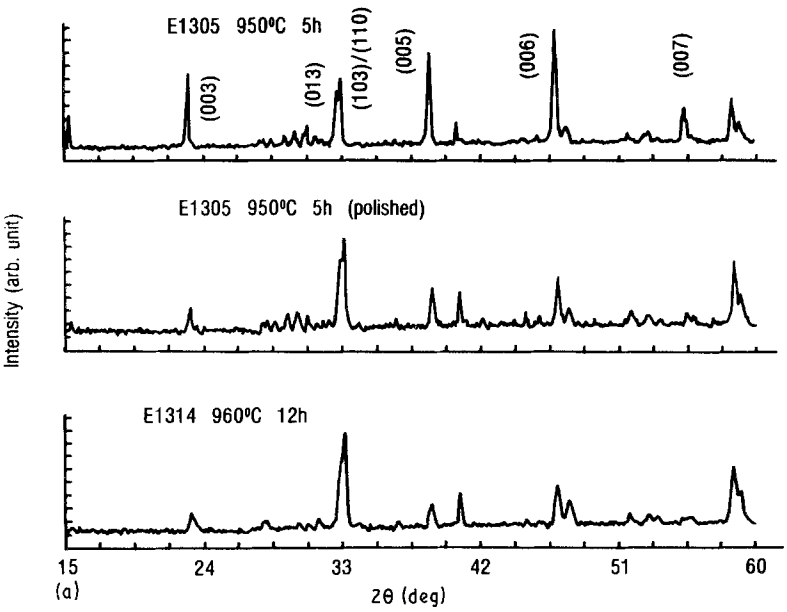

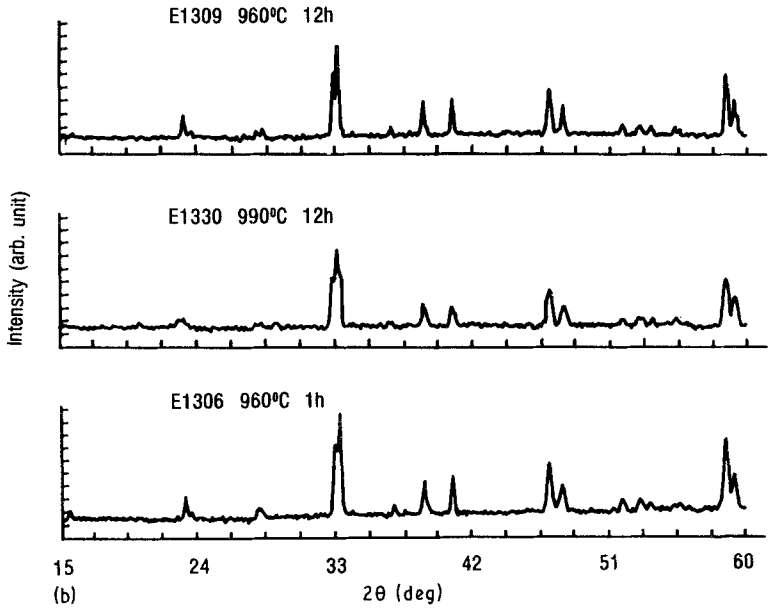

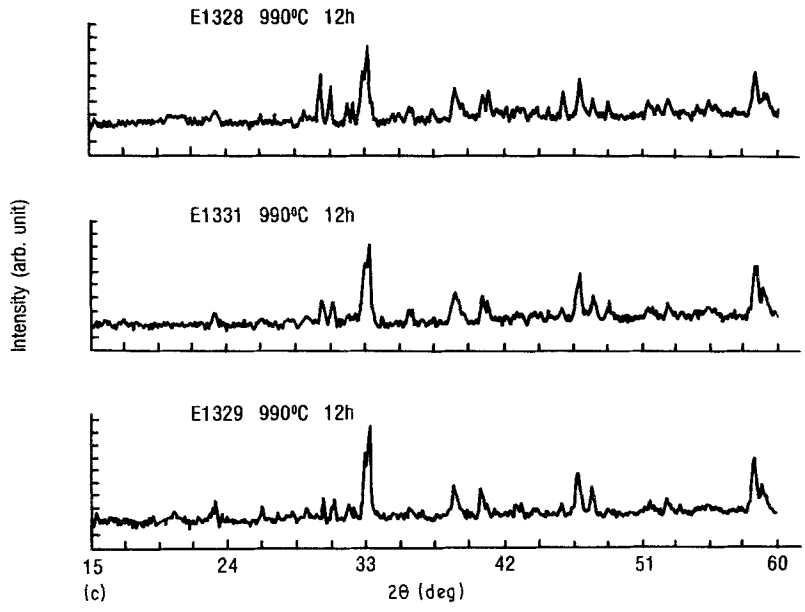

Figure 3 X-ray diffraction patterns of sintered disc samples: (a) Series A: $BaCO_3$ and cupric oxide combined with yttrium oxide (E1305) or yttrium oxalate (E1314). (b) Series B: $BaCO_3$ and cupric carbonate combined with yttrium oxide (E1309), yttrium carbonate (E1330) or yttrium oxalate (E1306). (c) Series C: $BaCO_3$ and cupric oxalate combined with yttrium oxide (E1328), yttrium carbonate (E1331) or yttrium oxalate (E1329).

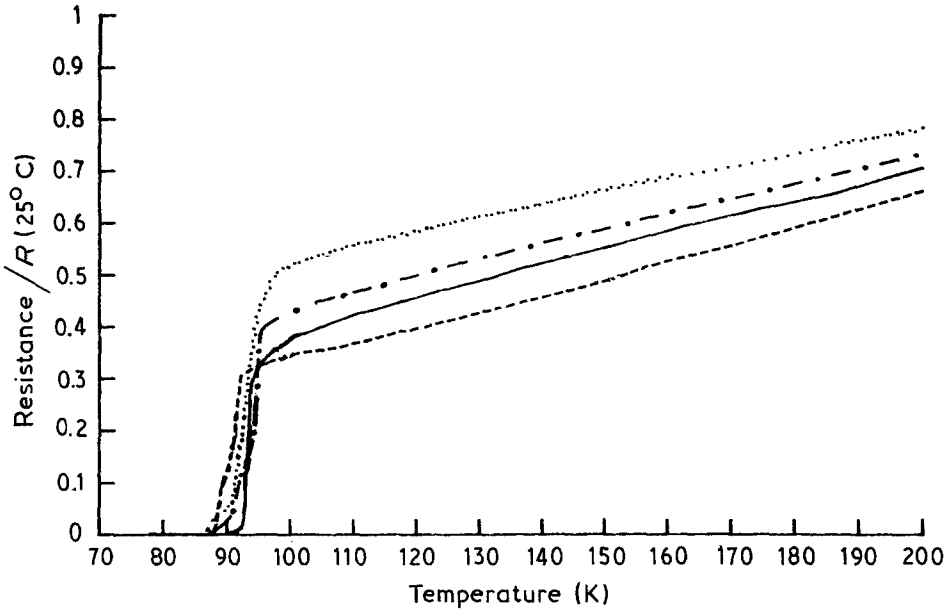

Figure 4 Normalized electrical resistance as a function of temperature for samples sintered at 990° C for 12 h: (····) E1305, (—·—) E1314, (——) E1306, (– – –) E1309.

shows the SEM micrographs of an as-sintered surface (Fig. 6a), a fracture surface in a dense sample (lot E1306) sintered at 990° C for 12 h with an Archimedes density of 6.03 g cm^{-3} (Fig. 6b), and a fracture surface of a less-dense sample (lot E1306) sintered at 960° C for 12 h with an Archimedes density of 5.85 g cm^{-3}. The as-sintered surface contained a mixture of equiaxed grains and elongated grains, which has the *c*-axis parallel to the short dimension. There was no apparent open porosity. However, approximately hemispherical pores were scattered in the fracture surfaces, with a greater amount of porosity in the less-dense sample. This would suggest that gas (probably CO_2) entrapment was mainly responsible for the internal porosity. There was no apparent enhancement in the grain size at the higher sintering temperature of 990° C. Thus, liquid-phase-assisted sintering was not observed.

The maximum densities achieved by the different powder lots are listed in Table II for samples sintered for 12 h at 990° C. The use of copper carbonate as the cupric source resulted in consistently high Archimedes densities of about 6.00 g cm^{-3}, or greater than 93% of the theoretical density. The use of copper oxalate in combination with Y_2O_3 or yttrium oxalate also gave high Archimedes densities between 5.70 and 5.93 g cm^{-3}, or between 90 and 93% of the theoretical density. In comparison, the use of CuO generally gave poor densities in the range of 60 to 70% of the theoretical density. These values were at the low end of the reported densities using CuO as the cupric source, probably due to the relatively simple powder processing method that was used in this evaluation.

The effect of sintering on the superconducting properties was investigated using the Meissner effect in the powder lot giving the highest density, E1306. Fig. 7 shows the magnetic susceptibility signal, normalized to sample weight, of samples sintered at 990° C. There is very little difference between sintering for 5 min (a geometrical density of 4.60 g cm^{-3}) and for 3 h (an Archimedes density of 5.78 g cm^{-3}) indicating that this bulk superconducting property is not dependent on the density. Other properties, such as critical current density, will be critically dependent on the density and crystal grain arrangement in the samples.

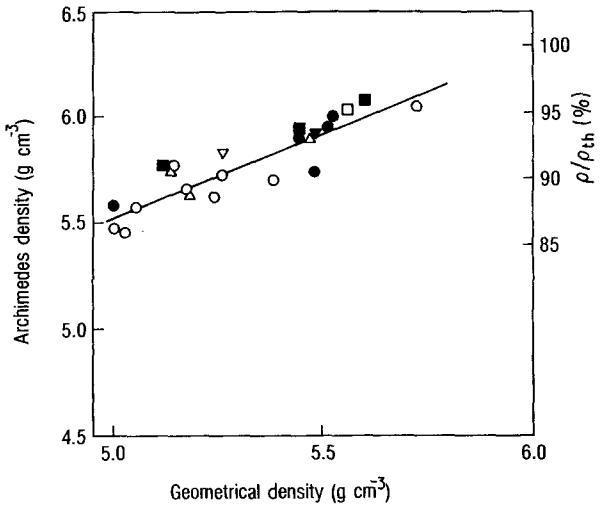

Figure 5 Plot of the Archimedes density against the corresponding geometrical density on samples of two different geometries and from four different powder lots. Disc, 15 000 psi (103.4 MPa): (△) E1309, (□) E1330, (○) E1306, (▽) E1328. Bar 24 000 psi (165.5 MPa): (■) E1330, (●) E1306, (▼) E1328.

TABLE II Maximum density achieved using different copper and yttrium sources (990° C, 12 h, O_2)

Powder lot	Density (g cm^{-3})	ρ/ρ_{th} (%)	Ion source
E1309	6.01*	94.6	Y oxide, Cu carbonate
E1330	5.92*	93.2	Y carbonate, Cu carbonate
E1306	6.03*	95.0	Y oxalate, Cu carbonate
E1328	5.93*	93.4	Y oxide, Cu oxalate
E1331	4.23†	66.6	Y carbonate, Cu oxalate
E1329	5.73*	90.2	Y oxalate, Cu oxalate
E1305	3.70†	58.3	Y oxide, Cu oxide
E1314	4.53†	71.3	Y oxalate, Cu oxide

*Archimedes density.
†Geometrical density.

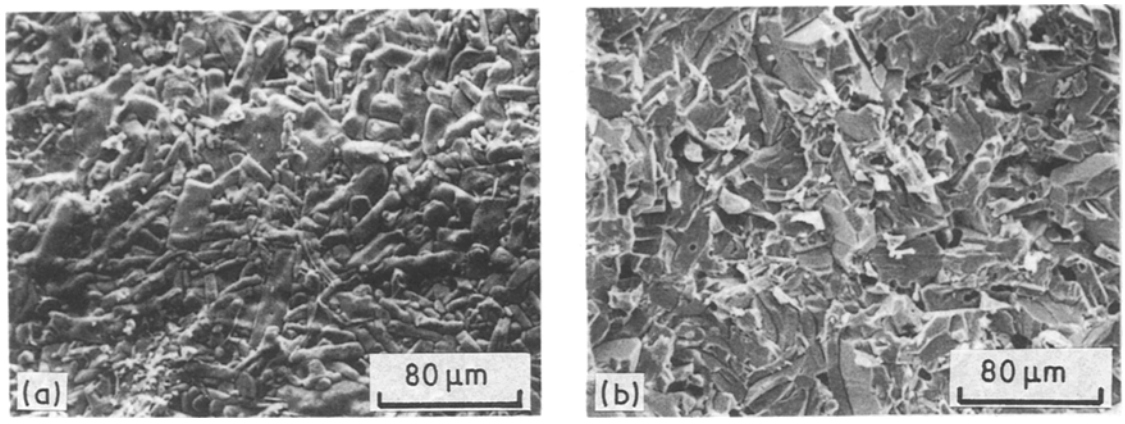

Figure 6 SEM micrographs of (a) as-sintered and (b) fractured surfaces of E1306 sample sintered at 990° C for 12 h and (c) fracture surface of another E1306 sample sintered at 960° C for 12 h (samples were 0.5 in. (1.27 cm) discs pressed at 15 000 psi (103.4 MPa)).

3.4. Linear shrinkage

A second useful parameter to monitor the densification behaviour is the linear shrinkage after sintering. Figs 8 and 9 show the linear shrinkage of disc samples as a function of sintering time for two sintering temperatures; 960 and 990° C. For all the powder lots, the shrinkage increased with the sintering time during the first 2 h, reaching a saturated value after about 4 to 6 h at the sintering temperature.

The figures illustrate the dramatic effect on densification of varying the starting cupric and yttrium sources. The use of cupric carbonate as the cupric source (lots E1309, 1306 and 1330) resulted in a rapid shrinkage in the first hour of sintering, reaching a saturated value of 16% at 960° C and 20% at 990° C. The maximum shrinkage corresponded to samples with the highest Archimedes density of 6.03 g cm^{-3} (ρ/ρ_{th} = 95%) achieved in lot E1306. There was a small effect exhibited by the use of different yttrium sources. In combination with cupric carbonate, yttrium oxalate and carbonate behaved similarly while yttrium oxide showed a slower densification rate at the shorter sintering times (< 3 h). However, the final shrinkage achieved was the same at long sintering times greater than 6 h.

The use of cupric oxalate as the cupric source resulted in a final shrinkage between 9 and 12% at 960° C and between 14 and 19% at 990° C. The largest shrinkage in this group was achieved by the combined use of yttrium oxide and cupric oxalate (lot E1328), corresponding to an Archimedes density of 5.93 g cm^{-3} (ρ/ρ_{th} = 93.4%). At 990° C, lot E1328 showed similar shrinkage behaviour to the powders lots using cupric carbonate as the cupric source.

The combined use of cupric oxide, yttrium oxide with barium carbonate (E1305) showed the least amount of densification. The linear shrinkage ranged from 0 to 5% for all sintering temperatures and times. This behaviour was similar for the two calcination conditions investigated: 900° C for 4 h followed by grinding with mortar and pestle, and 950° C for 16 h followed by 4 h ball-milling in isopropanol. Thus, the powder that was prepared from the solid-state reaction of $BaCO_3$, CuO and Y_2O_3 exhibited the lowest geometrical density of about 3.7 g cm^{-3}, or about 58% of theoretical density. X-ray diffraction analysis of the calcined powders showed a residue of $BaCO_3$ of 43.9% in the 900° C calcined powder compared with 2.4% in the 950° C calcined powder*. This ruled out the incomplete decomposition of $BaCO_3$ as the primary cause of the extremely low density in powder lot E1305. So far, the cause(s) have not been identified.

The use of yttrium oxalate with cupric oxide (E1314) gave a slightly better densification, with a total shrinkage of 8% at 960° C and 15% at 990° C. The highest geometrical density was 4.53 g cm^{-3}, or 71% of the theoretical density.

There was a linear relation between the dimensional shrinkage and the geometrical density (or Archimedes density), extending between 9 and 20% shrinkage. This is shown in Fig. 10 for two sample geometries: 0.5 in. (1.27 cm) disc pressed under 15 000 psi (103.4 MPa) and rectangular bar 0.125 in. × 0.5 in. (0.32 cm × 1.27 cm) pressed under 24 000 psi (165.5 MPa). The dashed line in the figure separates the data corresponding to the disc and bar samples. The slopes of the two curves were very similar, with a rate of increase in density of about 0.14 g cm^{-3} per 1% change in shrinkage. At the same shrinkage, the data for the bar samples were offset towards a greater density by approximately 0.59 g cm^{-3}. Thus, the linear shrinkage

*Percentage of $BaCO_3$ approximated by the ratio of the strongest $BaCO_3$ peak to the strongest combined $YBa_2Cu_3O_x$ peaks of (0 1 3), (1 0 3) and (1 1 0).

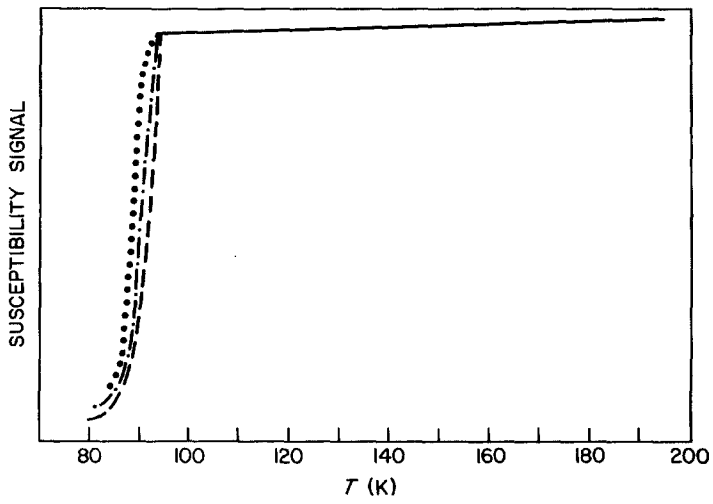

Figure 7 Magnetic susceptibility signal, normalized to sample weight, of E1306 sintered at 990° C for (····) 5 min, (—·—) 1 h and (– – –) 3 h.

was found to depend on the sample geometry and/or compaction pressure.

This dependence was further examined by maintaining the disc geometry while varying the diameter of the disc and the compaction pressure separately. Fig. 11 shows the geometrical density against linear shrinkage for three types of disc samples: (a) 0.5 in. (1.27 cm) diameter with a compaction pressure of 15 000 psi (103.4 MPa); (b) 0.25 in. (0.64 cm) diameter with a compaction pressure of 15 000 psi (103.4 MPa); and (c) 0.25 in. (0.64 cm) diameter with a compaction pressure of 24 000 psi (165.5 MPa). At the same shrinkage, the density was the largest in type (c) samples and smallest in type (a) samples. In each case, there was a linear correlation between the density and the shrinkage. The slopes for the three types of samples were 0.14, 0.17 and 0.19 g cm^{-3} per 1% change in shrinkage for type (a), (b) and (c) samples, respectively. At the same shrinkage, the disc samples with 0.25 in. diameter and pressed at 24 000 psi had higher densities than the samples pressed at 15 000 psi by about 0.20 to 0.32 g cm^{-3}. Similarly, the 0.25 in. disc samples had a higher density than the 0.5 in. disc samples compacted at the same pressure of 15 000 psi by about 0.40 g cm^{-3}. From the data in Figs 10 and 11, it is apparent that both the sample geometry (shape and size) and the compaction pressure gave separate contributions to the shrinkage.

3.5. General discussion

An important parameter that determines the final sintered density and shrinkage of compacted samples is the green density after compaction. It is anticipated that a higher green density will result in a smaller shrinkage during sintering and a higher sintered density. Table III lists the green densities measured for the three types of sample geometry and two compaction pressures. There was little difference between lots E1306 and 1309, both of which used cupric carbonate as the source of cupric ion. The highest green density of 3.61 g cm^{-3} was obtained for the 0.25 in. disc samples pressed at 24 000 psi, while the lowest green density of 3.19 g cm^{-3} was obtained for the 0.5 in. disc samples pressed at 15 000 psi. There was one-to-one

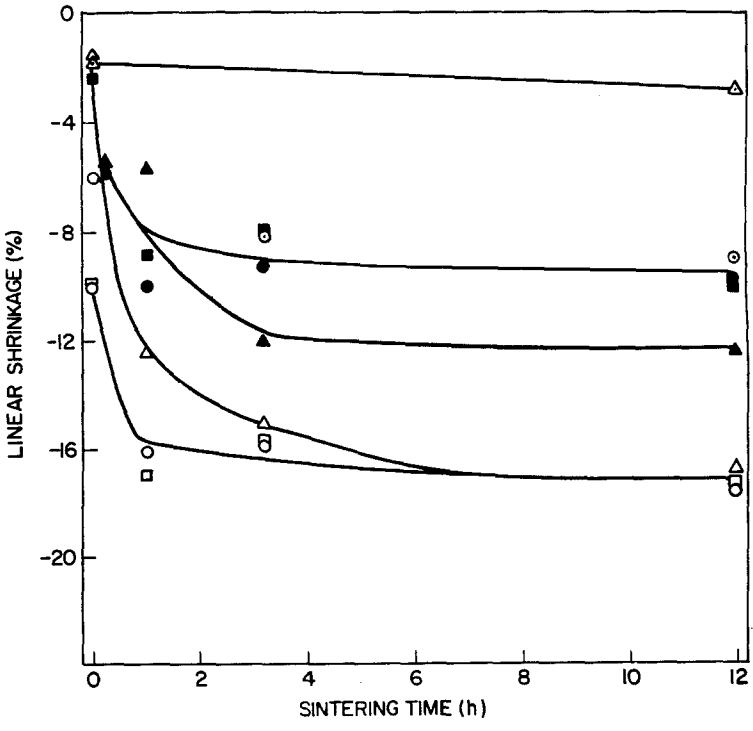

Figure 8 Linear sintering shrinkage of disc samples with a green diameter of 0.5 in. (1.27 cm) compacted at 15 000 psi (103.4 MPa) as a function of sintering time at the sintering temperature of 960° C: (△) E1305, (△) E1309, (▲) 1328, (⊙) E1314, (○) E1306, (●) E1329, (□) E1330, (■) E1331.

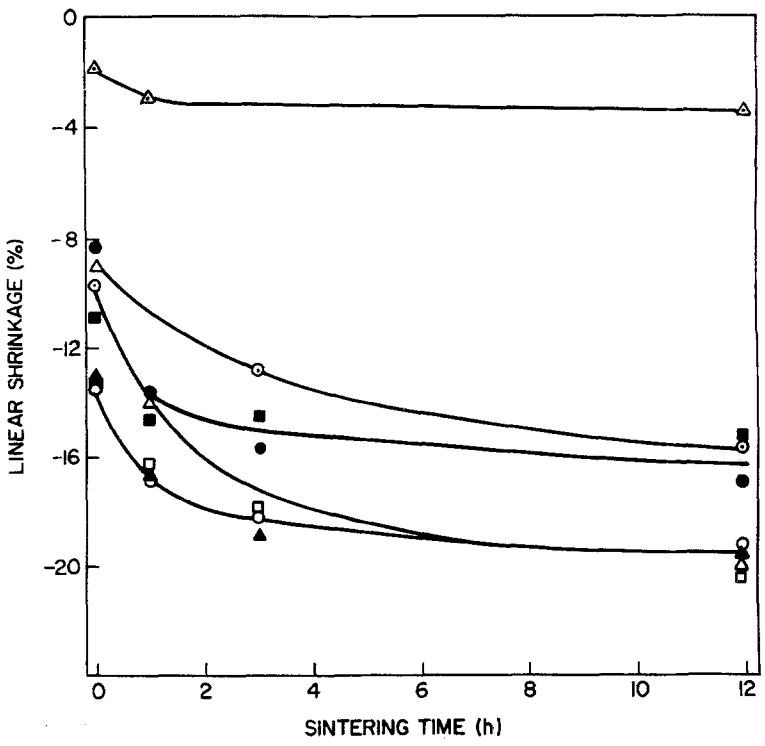

Figure 9 Linear sintering shrinkage of disc samples with a green diameter of 0.5 in. (1.27 cm) compacted at 15 000 psi (103.4 MPa) as a function of sintering time at the sintering temperature of 990° C: (△) E1305, (△) E1309, (▲) E1328, (⊙) E1314, (○) E1306, (●) E1329, (□) E1330, (■) E1331.

correspondence: higher green density resulted in higher sintered density. There was also a multiplying effect; the increase in sintered density was greater than the increase in green density between two types of sample. For example, the difference in green density between 0.25 in. and 0.5 in. discs compacted at the same pressure of 15 000 psi was 0.24 g cm^{-3}, but the difference in the sintered density was increased to about 0.40 g cm^{-3}. Similarly, while the difference in green density for 0.25 in. discs compacted at 24 000 and 15 000 psi was 0.19 g cm^{-3}, the difference in sintered density was increased to about 0.20 g cm^{-3} at small dimensional shrinkage (low sintering temperature and short sintering time) and to 0.32 g cm^{-3} at large dimensional shrinkage (higher sintering temperature and longer sintering time). These data illustrated the benefits of higher compaction pressure. An empirical relation between the green density and the compaction pressure is given by [15]

$$\rho_g = \rho_i + T\sigma^{1/3} \quad (1)$$

where ρ_g is the green density of the compacted sample, ρ_i is the density of the powder before compaction, σ is the stress along the length of the sample and T is a constant. The stress σ is a complicated function of the sample geometry (length and width) and powder properties, as well as the compaction pressure. Only compaction of powder into a disc geometry has been analysed [16–18]. It is reasonable to say that a higher compaction pressure will result in higher internal stresses, leading to higher green density, ρ_g. Furthermore, the higher internal stresses enhance the sintering process, leading to the multiplying effect in sintered density. The limitation of high compaction pressure is the occurrence of layer cracks in the green compacts, which may be alleviated by the use of appropriate lubricant or binder during the pressing operation.

The densification effect due to sample geometry and compaction pressure was also observed in lot E1305, which used cupric oxide as an ingredient, and lot E1328, which used cupric oxalate as an ingredient. However, a comparison between the green and sintered densities between the four lots (E1305, E1306, E1309 and E1328) suggested that other differences in the powders constituted a more important effect on the densification and sintered density. For example, E1328 had the highest green density among the four lots; but the shrinkage and sintered density at 960° C were smaller than for lots E1306 and 1309. On the other hand, the green density of lot E1305 was only about 5% smaller than for E1306, but the sintered density was significantly lower. Thus, the physical powder characteristics and the mechanics of compaction, measured collectively by the green density, were insufficient to account for the enhanced densification observed in powder lots using cupric carbonate as the cupric source. One possibility was enhanced surface diffusion during sintering, which

TABLE III Green density of compacted samples of different geometries

Sample	Density (g cm^{-3})			
	E1305	E1306	E1309	E1328
0.50 in. disc (15 000 psi)	3.070 ± 0.02	3.185 ± 0.01	3.192 ± 0.01	3.481 ± 0.01
0.25 in. disc (15 000 psi)	3.220 ± 0.01	3.410 ± 0.02	3.432 ± 0.02	3.768 ± 0.005
0.25 in. disc (24 000 psi)	3.454 ± 0.02	3.609 ± 0.03	3.620 ± 0.03	3.890 ± 0.005
Rectangular bar (24 000 psi)	3.318 ± 0.01	3.448 ± 0.02	3.445 ± 0.01	3.828 ± 0.01

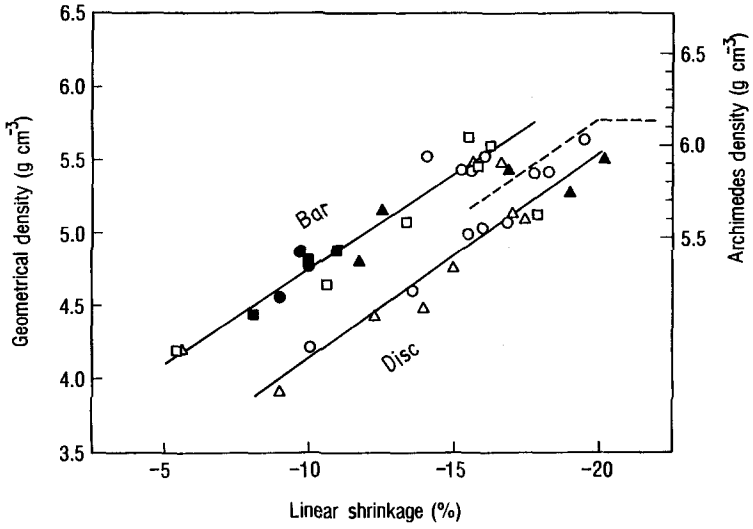

Figure 10 Geometrical and Archimedes densities as a function of linear sintering shrinkage for two sample geometries: 0.5 in. (1.27 cm) disc compacted at 15 000 psi (103.4 MPa) and rectangular bars compacted at 24 000 psi (165.5 MPa). (△) E1309, (▲) E1328, (○) E1306, (●) E1329, (□) E1330. (■) E1331.

would be affected to different degrees by the surface chemistry of powders prepared from different starting raw materials. Electron spectroscopy for chemical analysis (ESCA) of powder surfaces of lots E1305, 1309 and 1328 (Fig. 12) showed qualitative similarities between E1309 and E1328, which sintered to much greater density, but the ESCA spectrum was different in E1305, which did not sinter well. Specifically, split or satellite peaks were observed in Ba(3d3), Ba(3d5), O(1s), Y(3d) and Ba(4d) peaks in E1309 and 1328, but not in E1305. While the interpretation of these satellites is still not clear, they indicate some differences in the surface chemistry of the powder particles and lend some support to the conjecture of enhanced surface diffusion in the powder lots with greater sintered density.

4. Conclusion

The solid-state reaction method to form the superconducting oxide $YBa_2Cu_3O_x$ was studied. It was found that the addition of the cupric and yttrium components accelerated the decomposition of the $BaCO_3$ component. At a constant heating rate of 10° C min^{-1} in the TGA analysis, the temperature of complete decomposition, T_f, was lowered from greater than 1000° C in pure $BaCO_3$ to between 915 and 985° C. The effectiveness in decreasing T_f can be ranked in the order of oxalate, carbonate and oxide. The use of cupric carbonate as the cupric source also resulted in the formation of a single phase of the superconducting $YBa_2Cu_3O_x$, representing a small improvement over cupric oxide. With cupric oxalate as the source, a greater amount of second phases was formed. The effect of starting copper and yttrium sources on the densification of the superconducting $YBa_2Cu_3O_x$ ceramics was studied with respect to the variables of sintering temperature, sintering time, sample geometry and compaction pressure. The highest density achieved in this study was 6.03 g cm^{-3} (ρ/ρ_{th} = 95%) at 990° C and 5.85 g cm^{-3} (ρ/ρ_{th} = 92%) at 960° C. The source of cupric ion had the largest effect on densification. The use of cupric carbonate resulted in a consistently high Archimedes density of about 6.00 g cm^{-3} and a large dimensional shrinkage of about 20% at 990° C for 12 h. Using cupric oxalate also gave a high Archimedes density between 5.70 and 5.93 g cm^{-3} at 990° C. The use of cupric oxide gave the lowest density and smallest shrinkage, consistent with the results in the literature which generally use the solid-state reacted powder of $BaCO_3$, Y_2O_3 and CuO. Within the same powder lot, higher sintered density and smaller dimensional shrinkage were observed in samples with higher initial green density and compaction pressure. However, a comparison between the different powder lots indicated that the enhanced densification and higher density achieved by the use of

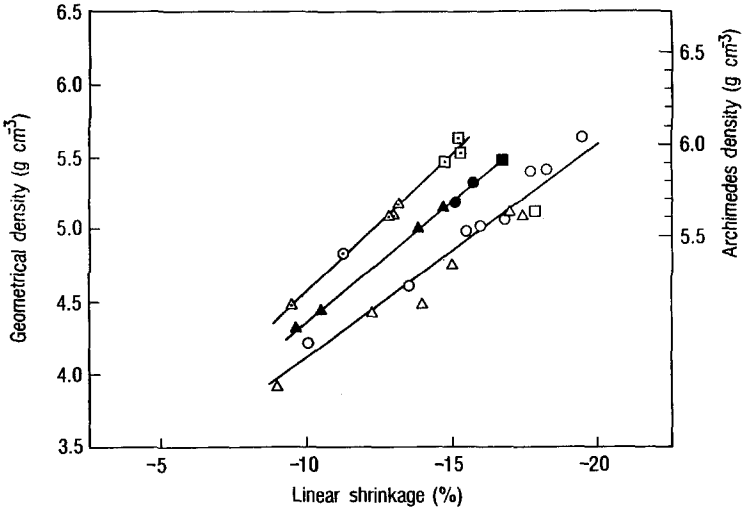

Figure 11 Geometrical and Archimedes densities as a function of linear sintering shrinkage for discs. 0.25 in. (0.64 cm) disc, 15 000 psi (103.4 MPa): (▲) E1309, (●) E1306, (■) E1330. 0.25 in. disc, 24 000 psi (165.5 MPa): (△) E1309, (○) E1306, (□) E1330. 0.5 in (1.27 cm) disc, 15 000 psi: (△) E1309, (○) E1306, (□) E1330.

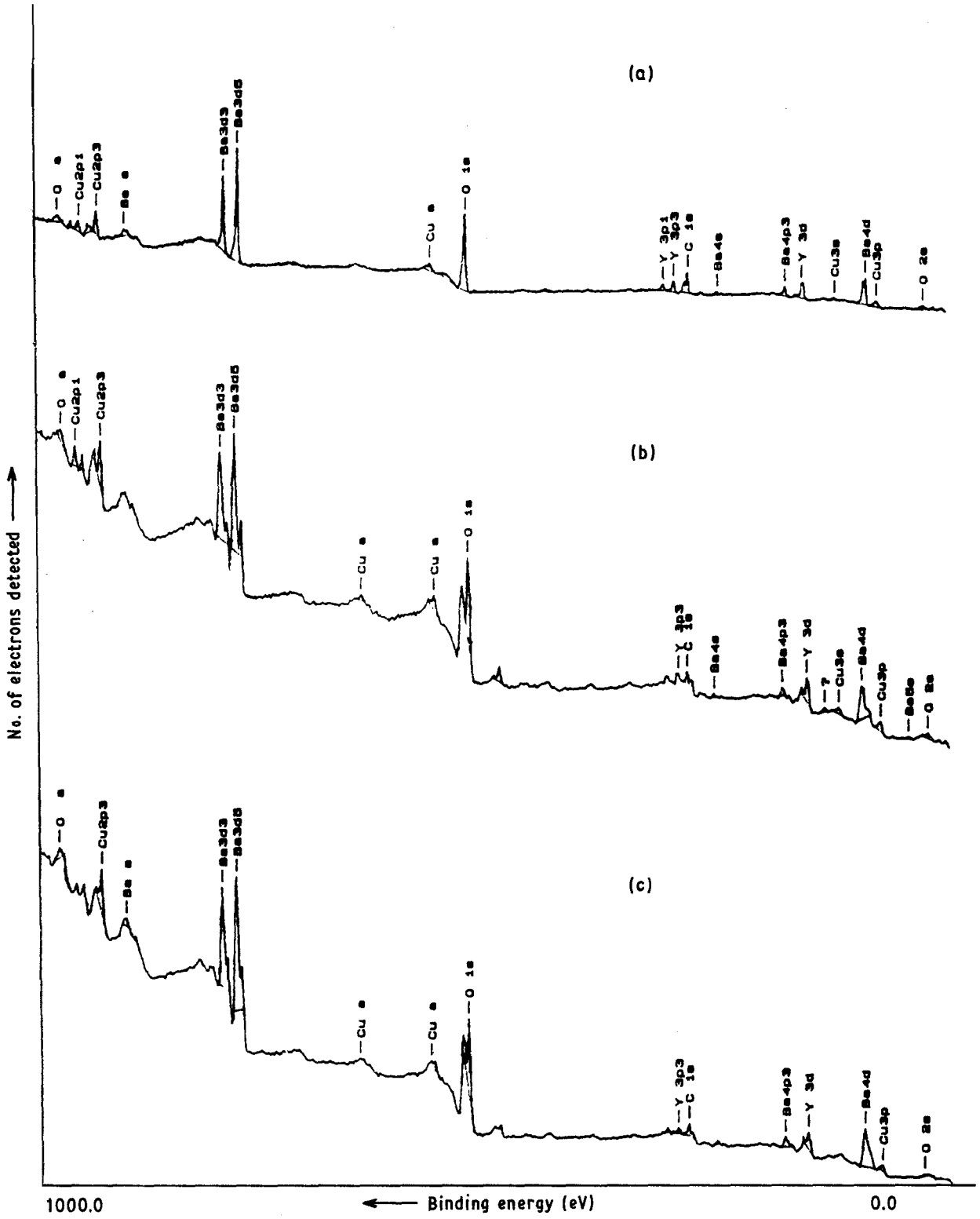

Figure 12 ESCA spectra of (a) E1305 (cupric oxide and yttrium oxide), (b) E1309 (cupric oxalate and yttrium oxide) and (c) E1328 (cupric oxalate and yttrium oxide), showing qualitative similarities between (b) and (c).

cupric carbonate cannot be accounted for by the different physical characteristics of the powders and the mechanics of powder compaction, measured collectively by the green density. One possible mechanism was enhanced surface diffusion during sintering, which would be affected by the surface chemistry of powders prepared from different starting raw materials.

Acknowledgements

The author wishes to thank G. S. Heyer and R. F. Roberts for performing the ESCA measurements.

References

1. D. W. JOHNSON Jr, E. M. GYORGY, W. W. RHODES, R. J. CAVA, L. C. FELDMAN and R. B. van DOVER, *Adv. Ceram. Mater.* **2** (1987) 329.
2. Q. ROBINSON, P. GEORGOPOULOS, D. L. JOHNSON, H. O. MARCY, C. R. KANNEWURF, S. J. HWU, T. J. MARKS, K. R. POEPPELMEIER, S. N. SONG and J. B. KETTERSON, *ibid.* **2** (1987) 386.
3. J. B. BLENDELL, C. K. CHANG, D. C. CRANMER, S. W. FREIMAN, E. R. FULLER Jr, E. DRESCHER-KRASICKA, W. L. JOHNSON, H. M. LEDBETTER, L. H. BENNETT, L. J. SWARTTZENDRUBER, R. B. MARINENKO, R. L. MYKLEBUST, D. S. BRIGHT

D. E. NEWBURY, *ibid.* **2** (1987) 512.
4. I. WEI CHEN, X. WU, S. J. KEATING, C. Y. KEATING, P. A. JOHNSON and T. Y. TIEN, *J. Amer. Ceram. Soc.* **70** (1987) C388.
5. P. K. GALLAGHER, H. M. O'BRYAN, S. A. SUNSHINE and D. W. MURPHY, *Mater. Res. Bull.* **22** (1987) 995.
6. H. TAKAGI, S. UCHIDA, H. SATO, H. ISHII, K. KISHIO, K. KITAZAWA, K. FUEKI and S. TANAKA, *Jpn J. Appl. Phys* **26** (1987) L601.
7. S. OHSHIMA and T. WAKIYAMA, *ibid.* **26** (1987) L812.
8. T. KAWAI and M. KANAI, *ibid.* **26** (1987) L736.
9. H. WATANABE, Y. KASAI, T. MOCHIKU, A. SUGISHITA, I. IGUCHI and E. YAMAKA, *ibid.* **26** (1987) L657.
10. D. G. HINKS, L. SODERHOLM, D. W. CAPONE, J. D. JORGENSEN and I. K. SCHULLER, *Appl. Phys. Lett.* **50** (1987) 1688.
11. R. C. BUDHANI, S. H. TZENG, H. J. DOERR and R. F. BUNSHAH, *ibid.* **51** (1987) 277.
12. H. M. O'BRYAN and J. THOMPSON, AT&T Bell Laboratories, unpublished data (1987).
13. B. BUNKER and J. VOIGT, presented at Spring Meeting of Materials Research Society, Reno, Nevada, 1988.
14. A. SAFARI, H. G. K. SUNDAR, A. S. RAO, C. WILSON, V. PARKHE, R. CARACCIOLO and J. B. WACHTMAN Jr, in Proceedings of 38th Electronic Components Conference, Los Angeles, 1988, pp. 181-187.
15. A. R. COOPER Jr and L. E. EATON, *J. Amer. Ceram. Soc.* **45** (1962) 97.
16. R. A. THOMPSON, *Amer. Ceram. Soc. Bull.* **60** (1981) 237.
17. *Idem, ibid.* **60** (1981) 244.
18. *Idem, ibid.* **60** (1981) 248.

Received 5 April
and accepted 4 September 1989